Research Square

Preprints are preliminary reports that have not undergone peer review.
They should not be considered conclusive, used to inform clinical practice,
or referenced by the media as validated information.

Flow-Dependent Growth and Decay of Precipitation over the Coastal–Orographic Zone of Padang, West Sumatra

Naila Az Zahra

nailaazzahra163@gmail.com

Sekolah Tinggi Meteorologi Klimatologi dan Geofisika

Adi Mulsandi

Sekolah Tinggi Meteorologi Klimatologi dan Geofisika

Research Article

Keywords: coastal convection, IMERG, orographic rainfall, semi-Lagrangian growth–decay, West Sumatra

Posted Date: June 12th, 2026

DOI: https://doi.org/10.21203/rs.3.rs-9918816/v1

License: This work is licensed under a Creative Commons Attribution 4.0 International License.
Read Full License

Additional Declarations: No competing interests reported.

Version of Record: A version of this preprint was published at Theoretical and Applied Climatology on October 15th, 2026. See the published version at https://doi.org/10.1007/s00704-026-06653-6.

Flow-Dependent Growth and Decay of Precipitation over the Coastal–Orographic Zone of Padang, West Sumatra

Naila Az Zahra[1*], Adi Mulsandi[1]

1Program Studi Meteorologi, Sekolah Tinggi Meteorologi Klimatologi dan Geofisika, Tangerang, 15119, Indonesia

Corresponding Author: nailaazzahra163@gmail.com

Abstract

This study investigates precipitation growth and decay (GD) over the Padang coastal–orographic region of western Sumatra during 2020–2024 using a semi-Lagrangian framework. Half-hourly IMERG Final Run V07B precipitation was combined with ERA5 850-hPa wind fields to estimate rainfall displacement and quantify intensity changes between origin and destination areas. ETOPO1 topography was used to interpret the influence of the coastline and the Bukit Barisan mountain range, while BMKG rain-gauge observations provided daily-scale observational support for IMERG rainfall accumulation. An event-scale analysis shows that rainfall maxima, growth regions, and decay regions do not always coincide spatially, highlighting the added value of the GD diagnostic. The multi-year mean GD is organized around the coastal–orographic transition, with positive GD generally appearing near the western coastal sector and weaker or negative GD occurring farther inland and around elevated terrain. The overall GD distribution is nearly balanced, with a weak positive mean but large variability. Westerly and southwesterly 850-hPa steering flows dominate the valid GD samples and produce the clearest coastal-to-inland GD contrast. However, fast-flow conditions tend to expand negative GD, suggesting that stronger advection may reduce the residence time of precipitation systems over the coastal–orographic zone. Positive GD also varies diurnally and seasonally. These findings indicate that precipitation evolution over Padang is governed by the combined effects of steering-flow direction, flow speed, land–sea contrast, diurnal timing, and orographic forcing.

Keywords: coastal convection; IMERG; orographic rainfall; semi-Lagrangian growth–decay; West Sumatra

1. Introduction

Precipitation over the Maritime Continent is governed by complex interactions among large-scale circulation, land–sea thermal contrast, coastal convergence, complex terrain, and local convective processes. These interactions are particularly important over Sumatra, where the elongated island geometry, direct exposure to the Indian Ocean, and the northwest–southeast-oriented Bukit Barisan Mountains create a sharp ocean–coast–mountain transition. Previous studies have

shown that rainfall over Sumatra exhibits a pronounced diurnal migration, with convective rainfall commonly developing over land and mountainous regions during the afternoon to evening and shifting toward coastal or offshore areas during the night to early morning (Mori et al., 2004; Marzuki et al., 2022a). This land–sea migration reflects the strong coupling between background flow, coastline geometry, and topographic forcing, making western Sumatra a key region for studying rainfall evolution in tropical coastal mountains.

The western coast of Sumatra is especially suitable for examining precipitation modification across a coastal–orographic environment. Padang lies on the western slope of the Bukit Barisan Mountains and directly faces the Indian Ocean, placing it within a narrow transition zone where maritime inflow, coastal convergence, and steep terrain interact over a relatively short horizontal distance. Observational studies in central western Sumatra have documented clear contrasts between coastal and inland rainfall characteristics, including the influence of lower-tropospheric zonal wind on coastal–inland rainfall distribution (Hamada et al., 2008). More recent studies have further shown that land–sea rainfall contrasts over Sumatra are expressed not only in rainfall amount and frequency, but also in rain-event propagation, diurnal timing, and vertical precipitation structure (Marzuki et al., 2022a; Marzuki et al., 2022b; Yusnaini et al., 2024). These findings indicate that precipitation over Sumatra should be interpreted not only as a spatial rainfall field, but also as an evolving system that responds to airflow, coastline, and terrain.

Despite these advances, many studies of rainfall over Sumatra still rely primarily on Eulerian diagnostics, such as rainfall amount, frequency, intensity, or vertical structure at fixed grid points or predefined regions. These diagnostics are useful for describing rainfall climatology, but they do not directly identify where a precipitating system intensifies or weakens as it moves across the ocean–coast–mountain continuum. This distinction is important because the location of maximum rainfall is not necessarily the same as the location of maximum precipitation growth. A rainfall maximum observed near the coast or mountain slope may reflect a system that intensified upstream at an earlier time and was subsequently advected into the observed location. Therefore, diagnosing rainfall evolution requires a framework that follows the estimated pathway of precipitating systems rather than only describing rainfall intensity at fixed locations.

A semi-Lagrangian growth–decay framework provides a useful approach for addressing this limitation. In contrast to a purely Eulerian perspective, which evaluates precipitation at fixed coordinates, a semi-Lagrangian approach estimates the upstream origin of a precipitating system and compares precipitation intensity between origin and destination areas. Previous precipitation growth–decay diagnostics have shown that this type of approach can reveal how rainfall evolution depends on flow direction, flow speed, topography, land–ocean boundaries, and diurnal variability (Kim et al., 2025). The framework is particularly relevant for regions where precipitation systems are strongly influenced by airflow and terrain interaction, because it

provides information beyond instantaneous rainfall intensity by identifying where precipitation systems tend to intensify or weaken along their estimated pathway.

In this study, the semi-Lagrangian growth–decay concept is adapted for the coastal–orographic region of Padang, West Sumatra, using satellite precipitation and reanalysis-derived flow. The Integrated Multi-satellite Retrievals for Global Precipitation Measurement (IMERG) provide high-frequency precipitation estimates over both land and ocean, allowing rainfall evolution to be examined across the Indian Ocean, coastal zone, and mountainous terrain. ERA5 provides hourly atmospheric flow fields that can be used to estimate the lower-tropospheric steering flow associated with precipitation displacement, while ETOPO1 represents the terrain contrast between the oceanic, coastal, and mountainous parts of the domain. This combination enables a process-oriented analysis of precipitation growth and decay over a region where long-term, spatially continuous precipitation observations with sufficient temporal coverage are limited. Because IMERG is a satellite-based product and ERA5 represents reanalysis-derived background flow, the results are interpreted as a diagnostic of satellite-derived precipitation evolution along estimated flow pathways, rather than as direct tracking of individual precipitation cells.

This study investigates flow-dependent precipitation growth and decay over Padang, West Sumatra, using IMERG precipitation, ERA5 850-hPa flow, and ETOPO1 topography within a semi-Lagrangian framework. The objectives are threefold: first, to identify the spatial distribution of precipitation growth and decay across the Indian Ocean–coast–Bukit Barisan transition; second, to examine how ERA5-derived flow direction and flow speed modulate the location and intensity of growth–decay patterns; and third, to evaluate the diurnal and monthly variability of positive precipitation growth over land and ocean. By focusing on precipitation evolution rather than rainfall intensity alone, this study provides a complementary framework for understanding rainfall modification in tropical coastal mountains and contributes to the broader understanding of rainfall predictability over western Sumatra.

2 Data and Methods

2.1 Study Area and Datasets

This study was conducted over Padang and its surrounding coastal–orographic region in West Sumatra, Indonesia. The analysis domain covers the transition from the Indian Ocean to the western coastal of Sumatra and the Bukit Barisan Mountains. This region is suitable for examining precipitation growth and decay because rainfall systems approaching the western coast of Sumatra may be modified by the land–sea boundary, coastal convergence, and orographic lifting along the western slope of the Bukit Barisan Mountains.

The study area is shown in Figure 1. Padang is located directly along the western coast of Sumatra and lies close to the steep terrain of the Bukit Barisan Mountains. This configuration produces a strong ocean–coast–mountain contrast within a relatively short horizontal distance, allowing precipitation evolution to be evaluated across a physically meaningful coastal–orographic gradient.

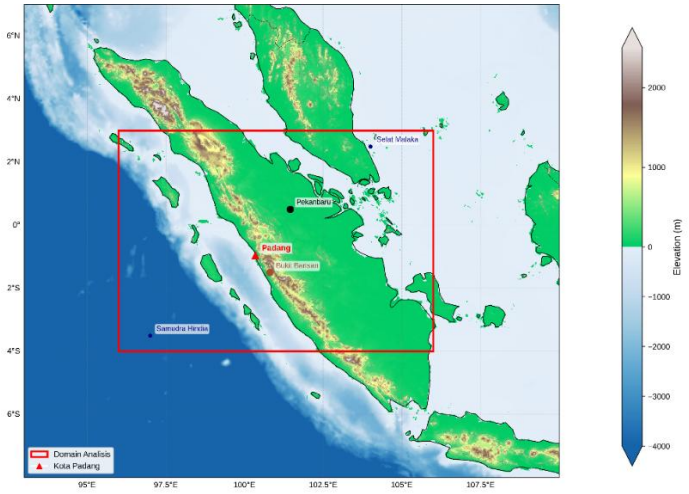


Figure 1. Study area and topographic characteristics of the Padang coastal–orographic region, West Sumatra. Elevation is derived from ETOPO1, and the analysis domain includes the Indian Ocean, the western coastal zone of Sumatra, Padang, and the Bukit Barisan Mountains.

This study used four datasets: IMERG precipitation, ERA5 atmospheric flow, ETOPO1 topography, and local daily rain-gauge observations from BMKG. IMERG was used as the primary precipitation dataset for calculating mean areal precipitation and growth–decay values. ERA5 was used to estimate the lower-tropospheric steering flow, flow direction, flow speed, and backward displacement. ETOPO1 was used to represent terrain elevation and the coastal–orographic setting. The BMKG rain-gauge data were used to evaluate the consistency of IMERG daily rainfall accumulation during the overlapping period. The datasets used in this study are summarized in Table 1.

Table 1. Datasets used for the semi-Lagrangian precipitation growth–decay analysis over the Padang coastal–orographic region.

Dataset	Variable used	Resolution	Period Used	Role in this study	Reference
GPM IMERG Final Run V07B	Precipitation rate	0.1°; 30 min	2020-2024	Calculation of MAP and GD	Huffman et al. (2020)
ERA5 pressure-level reanalysis	850-hPa u and v wind components	0.25°; hourly	2020-2024	Steering flow, backward displacement, flow direction, and flow speed	Hersbach et al. (2020)

ETOPO1 Ice Surface Global Relief Model	Surface elevation	1 arc-minute	Static	Terrain, coastline, and orographic interpretation	Amante and Eakins (2009)
BMKG local rain gauge	Daily Rainfall accumulation	Station based; daily	1991-2025; 2020–2024 overlap for daily comparison	Daily scale observational support for IMERG rainfall accumulation	BMKG Observational data

IMERG Final Run V07B was selected because it provides half-hourly precipitation estimates over both land and ocean, which are required to examine sub-daily precipitation evolution. The precipitation field was expressed as rainfall intensity in mm h^{-1}. ERA5 wind components at 850 hPa were selected to represent the lower-tropospheric background steering flow. This level was used to estimate precipitation displacement and classify flow regimes, but it is not interpreted as near-surface wind. ETOPO1 was used to describe the terrain contrast between the Indian Ocean, the coastal plain, and the Bukit Barisan Mountains. The BMKG rain-gauge record extends from 1991 to 2025, but only the 2020–2024 overlap with IMERG and ERA5 was used for daily-scale comparison. Because the gauge data are available as daily totals, they were used to evaluate daily rainfall accumulation rather than sub-daily or diurnal variability.

2.2 Daily-scale observational support using BMKG rain-gauge data

BMKG daily rain-gauge observations were used as daily-scale observational support for IMERG rainfall accumulation during the overlapping period of 2020–2024. Because the available gauge data are daily totals, the comparison was performed at the daily accumulation scale. Half-hourly IMERG precipitation estimates were accumulated into daily rainfall totals and compared with the corresponding BMKG daily rainfall observations at the nearest IMERG grid point.

This comparison was intended to assess the consistency of IMERG daily rainfall accumulation and to support event interpretation. It was not used to directly validate the 30-min growth–decay fields, because the temporal resolution of the rain-gauge observations is not equivalent to the sub-daily IMERG data. Therefore, the BMKG observations are treated as observational support for daily rainfall accumulation, while the semi-Lagrangian growth–decay analysis relies on the half-hourly temporal resolution of IMERG.

2.3 Semi-Lagrangian Growth–Decay Calculation

A semi-Lagrangian growth–decay framework was applied to estimate whether precipitation intensified or weakened along its estimated displacement pathway. In this study, IMERG precipitation was used to represent rainfall intensity, while ERA5 850-hPa wind was used to estimate the lower-tropospheric steering flow for backward displacement. This approach allows precipitation change to be evaluated along an estimated flow pathway rather than only at fixed grid points (Huffman et al., 2020; Hersbach et al., 2020; Kim et al., 2025).

For each destination grid point at the current time t, the corresponding origin point at the previous time $t - \Delta t$ was estimated using the ERA5 850-hPa horizontal wind vector:

$$\Delta x = V \Delta t$$

$$\boldsymbol{x}_{orig} = \boldsymbol{x}_{dest} - \Delta x$$

where Δx is the estimated displacement vector during the tracking interval, $\mathbf{x}_{dest}$ is the destination location at time t, $\boldsymbol{x}_{orig}$ is the estimated origin location at $t - \Delta t$, V is the ERA5 850-hPa horizontal wind vector, and Δt is the tracking interval. In this study, Δt was set to 1 h.

The backward-tracking procedure is illustrated in Figure 2 using a timestep from the 21 January 2021 case-study event at 11 UTC, corresponding to 18.00 WIB. This time lies within the 16.00–19.00 WIB period analyzed in the case-study figure. Figure 2 is used only to illustrate how the origin area is estimated from a destination area using ERA5 850-hPa flow; the full analysis applies the same procedure to all valid IMERG timesteps during 2020–2024.

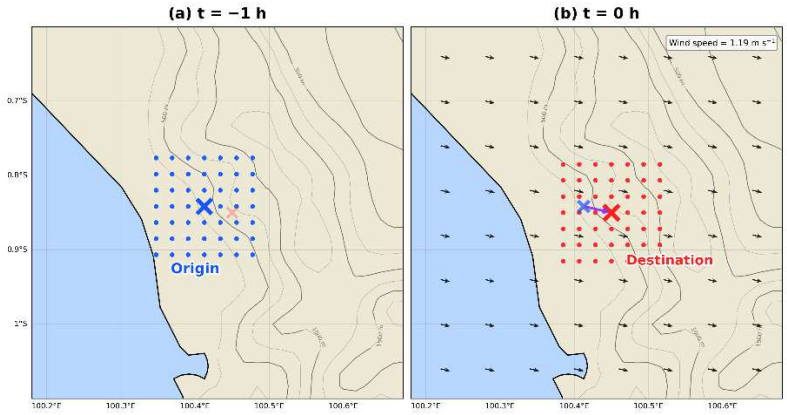


Figure 2. Example of the semi-Lagrangian backward-tracking procedure applied to the 07 March 2021 case-study event at 11 UTC (18.00 WIB). Blue points indicate the estimated origin sampling area at $t - 1$h, while red points indicate the destination sampling area at t. The blue and red crosses mark the centers of the origin and destination areas, respectively. The origin position is estimated from the destination position using the ERA5 850-hPa wind vector with a 1-h backward step. Black arrows in panel (b) show the ERA5 850-hPa flow used to estimate the displacement.

Mean areal precipitation was calculated at both the origin and destination areas using an equivalent 28-km spatial averaging window:

$$MAP = \frac{1}{N}\sum_{i=1}^{N} Pi$$

where MAP is the mean areal precipitation in mm h^{-1}, P_i is the precipitation intensity at grid point i, and N is the number of grid points within the averaging window.

Precipitation growth and decay were then quantified by comparing destination and origin MAP values:

$$GD = 10\, log_{10}\left(\frac{MAP_{dest} + c}{MAP_{orig} + c}\right)$$

where GD is the growth–decay value in dB, MAP_{dest} is the mean areal precipitation at the destination area, MAP_{orig} is the mean areal precipitation at the origin area, and $c$is a small constant used to avoid division by zero. In this study, $c = 0.01$mm h^{-1}. Positive GD indicates precipitation growth from the origin to the destination area, while negative GD indicates precipitation decay. Only samples with $MAP \geq 0.1$mm h^{-1} were included in the calculation to reduce the influence of near-zero rainfall values. For visualization purposes, precipitation and GD fields were lightly interpolated in the figures; however, all GD calculations and the identification of rainfall maxima, growth centers, and decay centers were performed on the native analysis grid.

2.4 Flow Classification and Composite Analysis

ERA5 850-hPa zonal and meridional wind components were used to represent the lower-tropospheric steering flow associated with each valid growth–decay sample. For each analysis time, the domain-mean wind components were calculated over the study area and used to derive flow speed and direction. Flow speed was calculated as

$$V = \sqrt{u^2 + v^2}$$

where V is the flow speed in m s^{-1}, u is the zonal wind component, and v is the meridional wind component.

Flow direction was calculated using the meteorological from-direction convention, in which direction denotes where the flow comes from rather than where it moves toward. The direction was defined as

$$\theta = \left(270° - atan2(v,u)\ x\ \frac{180}{\pi}\right)\ mod\ 360°$$

where θ is the meteorological flow direction in degrees, and $\mathrm{atan2}\ (v,u)$ is the two-argument arctangent function used to preserve the correct quadrant. The multiplication by $180°/\pi$ converts the arctangent result from radians to degrees, while the modulo operation constrains the direction to the $0° - 360°$ range.

The resulting directions were classified into eight 45° sectors: N, NE, E, SE, S, SW, W, and NW. Directional composites were then calculated by averaging valid GD samples assigned to each sector based on the domain-mean ERA5 850-hPa steering flow. The percentages shown in the direction-composite figure represent the relative frequency of valid GD samples in each directional sector.

For the flow-speed sensitivity analysis, only the two dominant flow regimes, W and SW, were considered. These samples were further separated into slow- and fast-flow categories using the median domain-mean 850-hPa flow speed calculated from the combined W and SW subset. The resulting threshold was 3.53 m s^{-1}. Slow-flow samples were defined as V < 3.53 m s^{-1}, whereas fast-flow samples were defined as V ≥ 3.53 m s^{-1}. This subset-based median threshold was used to provide a balanced separation of the dominant onshore and oblique-onshore flow regimes.

Composite analysis was applied to evaluate the spatial behavior of GD under different flow regimes. The mean GD field was first calculated using all valid samples at each grid point

$$\overline{GD}(x,y) = \frac{1}{M}\sum_{j=1}^{M} GD_j(x,y)$$

where $\bar{GD}(x,y)$is the mean GD value at grid point (x, y), $GD_j(x,y)$is the GD value for sample j, and $M$is the total number of valid samples at that grid point.

The same averaging procedure was then applied separately for each flow-direction sector and flow-speed category. For direction-based composites, each valid precipitation sample was assigned to one of the eight flow-direction sectors based on the domain-mean ERA5 850-hPa

steering flow. Therefore, the percentages shown in the direction-composite figures represent the relative frequency of valid precipitation growth–decay samples in each sector, not the frequency of all ERA5 wind samples. Both relative frequencies and absolute sample counts were reported for the directional and speed-based composites to indicate the robustness of each category. This distinction is important because the wind-rose distribution and the GD composite frequencies do not need to be identical, although their dominant flow regimes should remain physically consistent.

2.5 Diurnal, Monthly, and Land-Ocean Analysis

Temporal variability was evaluated using positive GD values only. Positive growth was defined as

$$GD_+ = GD, GD > 0$$

where GD_+ represents positive precipitation growth. Values of GD ≤ 0 were excluded from this specific analysis because the purpose was to evaluate the conditional intensity of precipitation growth events, rather than the full growth–decay distribution.

Diurnal variability was analyzed by grouping positive GD values according to local hour using Western Indonesian Time (WIB; UTC+7). For each local hour, the mean positive growth was calculated as

$$\overline{GD}_{+,h} = \frac{1}{K_h} \sum_{k=1}^{K_h} GD_{+,k}$$

where $\bar{GD}_{+,h}$ is the mean positive growth for local hour h, and K_h is the number of positive-growth samples within that hour. Monthly variability was analyzed by calculating the monthly mean positive GD for the full domain and separately over land and ocean grid points

$$\overline{GD}_{+,m} = \frac{1}{K_m} \sum_{k=1}^{K_m} GD_{+,k}$$

where $\bar{GD}_{+,m}$ is the mean positive growth for month m, and K_m is the number of positive-growth samples in that month.

Land and ocean grid points were classified using ETOPO1 elevation data. Grid points at or above sea level were treated as land, while grid points below sea level were treated as ocean. Therefore,

the hourly and monthly analyses represent the conditional mean intensity of positive growth events, not the frequency of rainfall occurrence. Because the land–ocean classification was applied on the 0.1° IMERG grid, coastal grid cells may represent mixed land–ocean conditions. Therefore, the land–ocean separation should be interpreted as a broad surface-type classification rather than a fine-scale coastline-resolving mask.

3. Results

3.1 Event-scale evolution of precipitation growth and decay

To demonstrate how the semi-Lagrangian growth–decay (GD) framework captures short-term precipitation evolution, an event-scale analysis was first performed before examining the multi-year composite patterns. This case-study analysis is intended to illustrate the separation between instantaneous rainfall intensity and the locations where precipitation actively intensifies or weakens along the estimated displacement pathway.

The selected event occurred on 7 March 2021, when two local BMKG rain-gauge stations in Kota Padang recorded heavy daily rainfall, with 127.0 mm day^{-1} at Tambang Semen Padang and 120.0 mm day^{-1} at Water Plan Semen Padang. The event was further screened using 30-min IMERG fields, which showed a coherent sub-daily rainfall evolution over the Padang coastal–orographic region from 18:00 to 21:00 WIB. This period was therefore selected to demonstrate the GD procedure under an organized rainfall episode supported by both local rain-gauge observations and satellite precipitation data.

Figure 3 presents the temporal evolution of IMERG precipitation intensity and the corresponding GD field during this event. The upper panels show the spatial distribution of rainfall intensity, while the lower panels show areas of precipitation growth and decay. During the event, the rainfall maximum, dominant growth center, and dominant decay center are not consistently collocated. This separation indicates that the GD field does not simply reproduce the instantaneous precipitation pattern, but provides additional information on where precipitation intensified or weakened between the estimated origin and destination areas.

At 18:00–20:00 WIB, the strongest precipitation is mainly concentrated over the northwestern part of the domain, whereas positive GD values occur over broader areas across the coastal–orographic transition zone. By 21:00 WIB, the rainfall maximum shifts southward, while the GD field shows a stronger positive signal over the southeastern part of the domain. This behavior indicates that the location of maximum rainfall intensity does not necessarily correspond to the location of active precipitation growth. Conversely, the decay centers identify areas where precipitation weakened along the estimated displacement pathway.

Overall, this case study illustrates the diagnostic value of the semi-Lagrangian GD framework. While the precipitation field identifies where rainfall occurred at each time, the GD field identifies

where rainfall strengthened or weakened along the estimated flow pathway. Therefore, Figure 3 serves as an event-scale demonstration before the analysis is extended to multi-year composite patterns in the following sections.

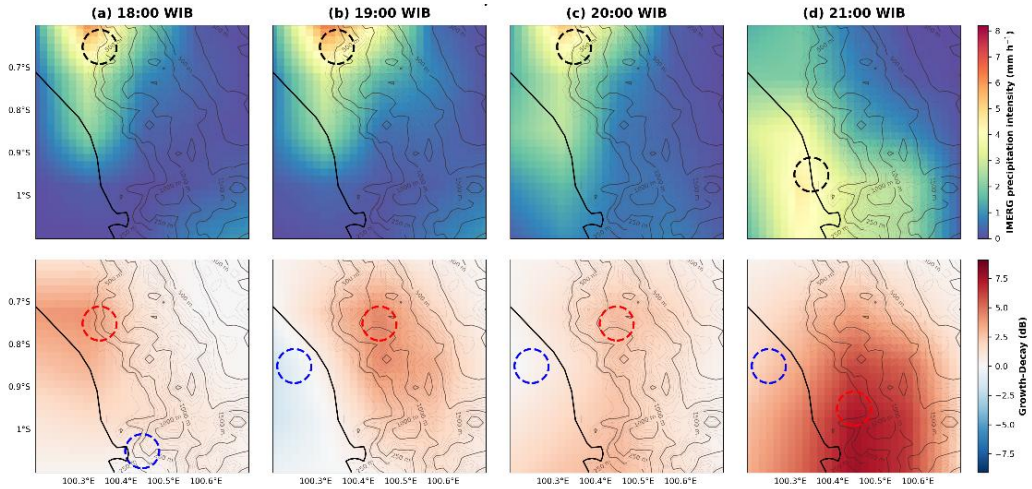


Figure 3. Temporal evolution of IMERG precipitation intensity and the corresponding growth–decay (GD) field over the Padang coastal–orographic region on 7 March 2021 from 18:00 to 21:00 WIB. Panels (a–d) show IMERG precipitation intensity, while panels (e–h) show the retrieved GD field. Black dashed circles mark rainfall maxima, whereas red and blue dashed circles indicate the dominant growth and decay centers, respectively. Topographic contours are derived from ETOPO1.

3.2 Mean Spatial Pattern of Precipitation Growth and Decay

The event-scale analysis in Section 3.1 demonstrates that rainfall intensity maxima do not necessarily coincide with the locations of precipitation growth and decay. To examine whether this behavior is also evident in the multi-year mean state, the spatial distribution of mean GD was analyzed for 2020–2024 and compared with the topographic structure of the Padang coastal–orographic region.

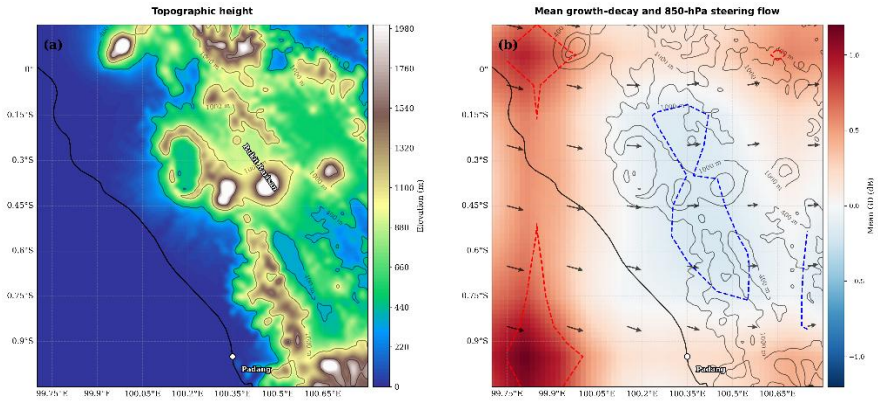


Figure 4. Topographic setting and mean growth–decay (GD) pattern over the Padang coastal–orographic region during 2020–2024. Panel (a) shows ETOPO1 topographic height, while panel (b) shows mean GD derived from IMERG precipitation using the semi-Lagrangian framework. Shading in panel (b) indicates mean GD in dB, arrows represent the mean ERA5 850-hPa steering flow, and dashed red and blue contours indicate the 90th and 10th percentile thresholds of mean GD, respectively.

Figure 4a shows the steep coastal–mountain transition associated with the Bukit Barisan range. The terrain rises rapidly from the western coastal plain toward the inland mountainous region, producing a sharp elevation gradient within a relatively short horizontal distance. This configuration provides a favorable setting for strong spatial modulation of precipitation as low-level flow interacts with the coastal boundary and the orographic slope.

The mean GD field in Figure 4b shows that precipitation growth and decay are not distributed uniformly across the domain. Positive mean GD values are more apparent over the western coastal sector and parts of the western slope region, while weaker or negative GD values appear around the elevated terrain and the central–eastern part of the domain. The mean GD statistics also indicate an asymmetric distribution, with a domain-mean value of approximately 0.27 dB and stronger positive anomalies than negative anomalies. The 90th percentile of mean GD reaches about 0.89 dB, whereas the 10th percentile is approximately −0.16 dB, suggesting that multi-year averaged growth signals are more pronounced than decay signals in this domain.

The spatial contrast between the positive and negative GD regions suggests that precipitation evolution is organized around the coastal–orographic transition rather than simply following the highest terrain. The positive GD signal along the western part of the domain is consistent with the tendency for precipitation to intensify as moist low-level flow approaches the coastal and upslope region. In contrast, the weaker or negative GD areas over and downstream of the elevated terrain indicate regions where precipitation tends to weaken after being advected across the terrain gradient. Therefore, the mean GD pattern reflects the combined influence of low-level steering flow, coastal geometry, and orographic modulation.

The ERA5 850-hPa vectors in Figure 4b provide additional context for this interpretation. The vectors represent the lower-tropospheric steering flow used in the semi-Lagrangian displacement estimate, not a direct tracking of individual rain cells. Under this framework, the GD field identifies where precipitation statistically strengthens or weakens between the estimated origin and destination areas. Thus, Figure 4 supports the use of the GD diagnostic as a complement to conventional precipitation intensity maps, because it highlights the spatial tendency of rainfall evolution rather than only the location of rainfall occurrence.

Overall, the multi-year mean pattern indicates that the Padang coastal–orographic region exhibits a persistent spatial organization of precipitation growth and decay. The strongest mean growth signals occur near the coastal–orographic transition, while decay signals are more localized and generally weaker. This result suggests that the interaction between low-level flow and the steep Bukit Barisan topography plays an important role in modulating the spatial evolution of precipitation over western Sumatra.

3.3 Statistical distribution of growth–decay and steering flow

Before examining the directional modulation of precipitation growth and decay, it is necessary to evaluate the overall statistical behavior of the GD field and the associated lower-tropospheric steering flow. This step provides a quantitative basis for determining whether the semi-Lagrangian GD values are centered around a neutral state or whether they exhibit a systematic tendency toward either precipitation growth or decay.

The distribution of all valid GD values during 2020–2024 is shown in Figure 5a. The mean GD is 0.18 dB, while the standard deviation is 4.16 dB. This sample-based mean differs from the domain-mean value of the multi-year mean GD field reported in Figure 4 because the former is calculated from all valid grid-scale GD samples, whereas the latter is obtained after temporal compositing at each grid point. These values were computed directly from all grid-scale GD samples that satisfied the semi-Lagrangian validity criteria, including the origin–destination overlap and the minimum mean areal precipitation threshold. The mean value represents the average tendency of precipitation intensity change between the origin and destination areas, whereas the standard deviation describes the spread of individual GD values around this mean state. The small positive mean indicates a weak overall tendency toward precipitation growth, but its magnitude remains close to zero. Therefore, the multi-year GD distribution suggests that growth and decay are broadly balanced when all valid samples are considered together.

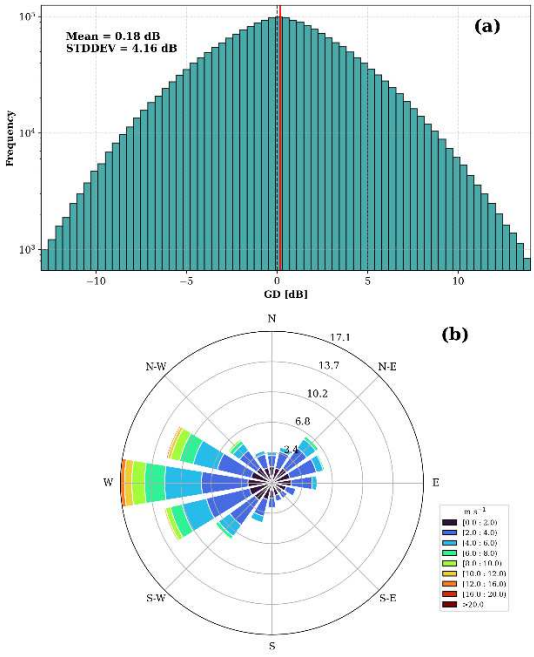


Figure 5. Statistical characteristics of semi-Lagrangian growth–decay (GD) values and ERA5 850-hPa steering flow over the Padang coastal–orographic region during 2020–2024. Panel (a) shows the frequency distribution of all valid GD values, with the dashed black line indicating GD = 0 dB and the red line indicating the mean GD. Panel (b) shows the wind rose of domain-mean ERA5 850-hPa steering flow for timesteps with valid GD samples, using the meteorological from-direction convention.

Despite the near-neutral mean, the relatively large standard deviation indicates substantial event-to-event and grid-to-grid variability. In physical terms, this means that the rainfall systems over the Padang coastal–orographic region do not evolve uniformly. Some samples experience pronounced intensification, while others undergo strong weakening after being advected by the 850-hPa steering flow. The logarithmic frequency scale also shows that extreme positive and negative GD values occur less frequently than values near zero, but they remain part of the distribution. This behavior is consistent with the intermittent nature of convective rainfall in complex coastal–orographic terrain, where local moisture convergence, terrain interaction, and flow direction can produce rapid changes in precipitation intensity.

The steering-flow distribution in Figure 5b provides the dynamical context for these GD variations. The wind rose was calculated from the domain-mean ERA5 850-hPa flow at timesteps with valid GD samples, using the meteorological from-direction convention. Therefore, a westerly sector indicates flow coming from the west and moving eastward toward the coastal and mountainous region. The distribution shows that westerly flow is the dominant regime associated with valid

GD samples, with additional contributions from southwesterly and northwesterly sectors. This indicates that many precipitation systems included in the GD analysis were associated with low-level flow from the Indian Ocean toward western Sumatra.

The wind-speed statistics further show that most valid GD samples occurred under weak to moderate steering flow. The mean speed is 3.38 m s^{-1}, the median is 2.81 m s^{-1}, and the 90th percentile reaches 6.55 m s^{-1}, while the maximum speed is 17.23 m s^{-1}. This indicates that the dominant rainfall evolution was not generally associated with very strong synoptic-scale flow, but rather with moderate steering conditions that can still advect precipitation systems across the coastal–orographic gradient. The presence of higher-speed samples, particularly within the westerly sector, suggests that stronger onshore flow events may occasionally contribute to more organized precipitation displacement and sharper growth–decay contrasts.

Overall, Figure 5 indicates that the GD distribution is nearly centered around zero but remains highly variable, while the valid GD samples are preferentially associated with westerly to southwesterly lower-tropospheric flow. This result provides the statistical basis for the directional composite analysis in the following section, where the spatial pattern of GD is examined separately for each steering-flow regime.

3.4 Directional modulation of precipitation growth and decay

The statistical distribution in Section 3.3 indicates that valid GD samples are most frequently associated with westerly to southwesterly lower-tropospheric flow. However, the frequency distribution alone does not show how precipitation growth and decay are spatially organized under each flow regime. Therefore, the GD field was further composited according to the ERA5-derived 850-hPa flow direction to examine whether different steering-flow regimes produce distinct growth–decay patterns over the Padang coastal–orographic region.

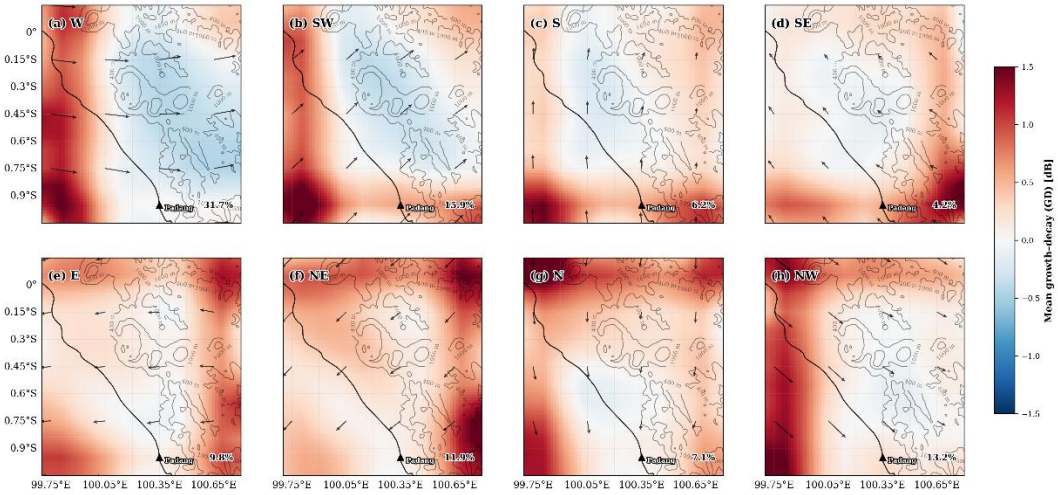


Figure 6. Mean growth–decay (GD) composites classified by ERA5-derived 850-hPa flow direction over the Padang coastal–orographic region during 2020–2024. Shading indicates mean GD in dB, arrows represent the mean ERA5 850-hPa steering vector for each directional sector, and contours show ETOPO1 topography. Percentages indicate the fraction of valid GD samples assigned to each flow direction; absolute sample counts are reported in the text.

Figure 6 shows that the spatial pattern of GD varies clearly among the eight directional sectors. The directional composite was based on 56,101 valid samples. Westerly flow contributes the largest fraction, accounting for 31.7% of the total samples (n = 17,758). This is followed by southwesterly flow at 15.9% (n = 8,911), northwesterly flow at 13.2% (n = 7,378), and northeasterly flow at 11.9% (n = 6,675). The remaining sectors contribute smaller fractions, with easterly, northerly, southerly, and southeasterly flows accounting for 9.8% (n = 5,516), 7.1% (n = 4,003), 6.2% (n = 3,493), and 4.2% (n = 2,367), respectively. These values indicate that the most common valid GD conditions are associated with flow from the western side of the domain, particularly from the Indian Ocean sector toward the western coast of Sumatra.

Under westerly and southwesterly flow, positive GD values are concentrated along the western side of the domain, especially near the coastal sector and the upstream side of the Bukit Barisan topographic barrier. In contrast, negative or weaker GD values appear farther inland and around the central elevated terrain. This pattern is physically consistent with onshore lower-tropospheric flow advecting moist precipitation systems from the Indian Ocean toward the coastal–orographic transition. As the systems move inland, the interaction with steep terrain and changes in local convergence may favor rainfall intensification on the upstream side, while weakening can occur over or beyond the more elevated terrain. The pattern does not imply that topography alone controls GD, but rather that flow direction and terrain geometry jointly modulate where precipitation tends to grow or decay.

The southerly and southeasterly composites show lower sample frequencies and more localized GD structures. In these regimes, positive GD appears mainly toward the southern and southeastern parts of the domain, while the central mountainous region remains closer to neutral or weakly negative. Because these sectors have smaller sample contributions, especially the southeasterly sector at 4.2%, their spatial patterns should be interpreted as less robust than the westerly and southwesterly composites. Nevertheless, they indicate that when the steering flow approaches the terrain from a more meridional or oblique direction, the growth–decay pattern shifts away from the dominant west–east coastal gradient.

For easterly and northeasterly flow, the composites show a different organization. Positive GD tends to appear over the northern, eastern, or boundary-side portions of the domain, while weaker or near-neutral values are found around parts of the central terrain. This contrast with the westerly composite suggests that the spatial tendency of precipitation evolution is sensitive

to the direction from which rainfall systems approach the coastal–orographic zone. Under easterly or northeasterly steering, the precipitation systems are not primarily advected from the Indian Ocean side toward the coastal slope, so the growth–decay pattern becomes less aligned with the western coastal transition.

The northwesterly composite also shows a relatively large contribution, at 13.2%, and retains a positive GD signal along the western side of the domain. This suggests that oblique onshore flow can still support precipitation growth near the coastal sector, although the spatial pattern is not identical to the purely westerly case. The result reinforces the interpretation that the western coastal boundary and Bukit Barisan terrain act as a preferred zone for precipitation modification when the lower-tropospheric flow contains an onshore component.

Overall, Figure 6 demonstrates that precipitation growth and decay over the Padang coastal–orographic region are directionally dependent. Westerly and southwesterly steering flows are the most frequent regimes associated with valid GD samples and show the clearest coastal-to-inland contrast in GD. Other directions produce more localized or weaker patterns, reflecting differences in how the steering flow intersects the coastline and orographic barrier. These results support the interpretation that precipitation evolution in this region is not only determined by rainfall intensity itself, but also by the interaction between low-level flow direction, coastal geometry, and the steep topographic gradient of western Sumatra.

3.5 Sensitivity of precipitation growth–decay to steering-flow speed and temporal variability

Beyond the directional dependence discussed in the previous section, the intensity and spatial organization of precipitation growth–decay are also affected by the speed of the steering flow. To examine this effect, the two dominant flow regimes, westerly and southwesterly, were further separated into slow- and fast-flow categories using the median domain-mean 850-hPa flow speed threshold of 3.53 m s^{-1}.

The W–SW subset contained 24,033 valid samples. Within this subset, W fast-flow conditions contributed the largest fraction (n = 9,701; 40.4%), followed by W slow-flow (n = 6,813; 28.3%), SW slow-flow (n = 5,063; 21.1%), and SW fast-flow (n = 2,456; 10.2%).

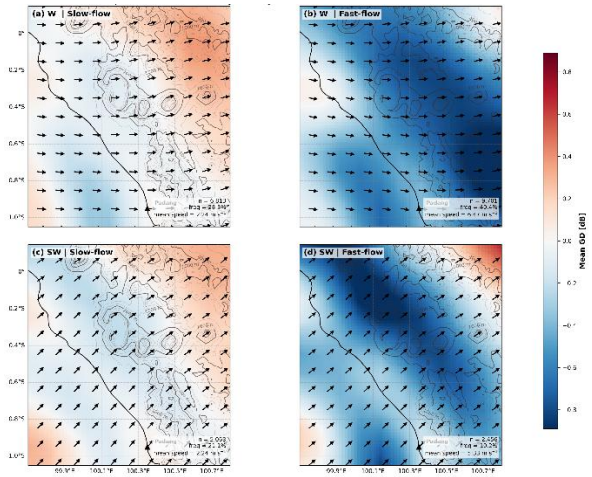


Figure 7. Mean growth–decay (GD) composites under dominant westerly (W) and southwesterly (SW) steering-flow regimes during 2020–2024, separated into slow- and fast-flow categories using the median domain-mean 850-hPa flow speed threshold of 3.53 m s^{-1}. Shading indicates mean GD in dB, arrows show the mean ERA5 850-hPa steering-flow direction, and contours indicate ETOPO1 terrain elevation. The sample size, frequency, and mean flow speed for each category are shown in each panel.

Figure 7 shows that the spatial structure of GD changes substantially between slow- and fast-flow conditions. Under slow westerly flow, the GD field exhibits a mixed pattern, with weak positive values over parts of the inland and northeastern sector and negative values over parts of the coastal–orographic corridor. A similar mixed structure is also seen under slow southwesterly flow. These patterns indicate that when the steering flow is relatively weak, precipitation systems may interact more gradually with the coastal and mountainous terrain, allowing both growth and decay to occur within the domain.

In contrast, the fast-flow composites show a broader and more coherent negative GD signal. This is particularly evident under westerly fast-flow conditions, where negative GD extends across much of the central and eastern part of the domain. The southwesterly fast-flow composite also shows expanded negative GD over the central coastal–orographic corridor, while positive values are more limited and mainly appear near the northeastern boundary. Therefore, these composites do not support a simple interpretation that stronger flow always enhances precipitation growth. Instead, stronger steering flow appears to favor more extensive weakening in this region, possibly because faster advection reduces the residence time of precipitation systems over the coastal–orographic zone.

This result is important because it refines the interpretation of the directional composites. Westerly and southwesterly flows are the most frequent regimes associated with valid GD samples, but their impact depends on flow speed. Under slower conditions, the GD pattern

remains spatially mixed, whereas faster flow tends to sharpen the contrast and expand the decay signal. Thus, the role of low-level flow is twofold: the flow direction controls how precipitation systems approach the coastline and terrain, while the flow speed modulates how long these systems can interact with the coastal–orographic environment.

The temporal variability of positive precipitation growth is summarized in Figure 8. Unlike Figures 4–7, which examine mean GD or directional composites, Figure 8 considers only positive GD values. Therefore, the figure represents the conditional intensity of growth events, not the frequency of rainfall occurrence. The hourly mean growth for all positive samples shows clear diurnal variability, with stronger growth generally occurring from late morning to afternoon. The most prominent peaks appear around 12:00 and 15:00 local time, when mean growth exceeds 4 dB. Lower values are observed during several early-morning hours, indicating that positive growth intensity is not uniform throughout the day.

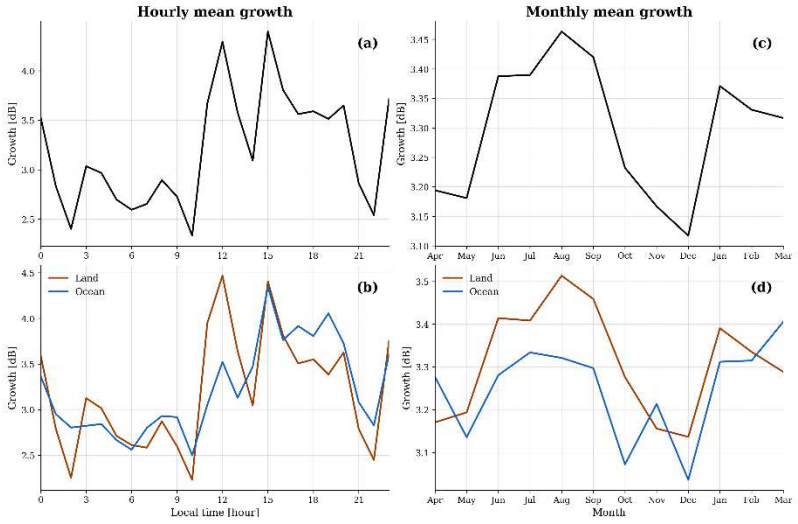


Figure 8. Temporal variability of positive precipitation growth (GD > 0) over the Padang coastal–orographic region during 2020–2024. (a) Mean hourly growth for all positive GD samples. (b) Mean hourly growth separated into land and ocean sectors. (c) Mean monthly growth for all positive GD samples. (d) Mean monthly growth separated into land and ocean sectors. Values represent the conditional mean intensity of positive GD events.

The land–ocean separation further shows that the diurnal growth signal differs between surface types. Land growth reaches a pronounced peak around midday, consistent with stronger daytime heating and enhanced convective development over land. Ocean growth is generally less sharply peaked at midday but remains relatively high during parts of the afternoon to evening period. This indicates that the timing of growth over land and ocean is not identical. Over land, growth is more directly linked to daytime heating and orographic enhancement, whereas over the adjacent ocean, growth may remain active later in the day as coastal and offshore circulations evolve.

Monthly variability is also evident in the positive-growth intensity. The full-domain monthly mean growth reaches its highest value around August, while the weakest value occurs around December. This indicates that the background environment modulating precipitation growth changes seasonally, even though positive growth occurs throughout the year. When separated by surface type, land growth is generally stronger during the mid-year months, especially from June to September, whereas ocean growth becomes comparable to or stronger than land growth during parts of the later wet-season period, including March. This seasonal contrast suggests that land-based convective enhancement and oceanic growth processes vary in relative importance across the annual cycle.

Overall, Figures 7 and 8 show that precipitation growth–decay over the Padang coastal–orographic region is not controlled by flow direction alone. Flow speed modifies whether the dominant westerly and southwesterly regimes favor mixed growth–decay patterns or broader weakening, while diurnal and monthly variability regulate when positive growth becomes most intense. These results indicate that precipitation evolution in western Sumatra is shaped by the combined effects of steering-flow direction, flow speed, land–sea contrast, and the timing of convective development.

4. Discussion

The results demonstrate that precipitation evolution over the Padang coastal–orographic region cannot be fully explained by rainfall accumulation alone. By applying a semi-Lagrangian growth–decay (GD) framework, this study evaluates how precipitation intensity changes along an estimated lower-tropospheric flow pathway. This approach provides a different perspective from conventional rainfall analysis because it distinguishes the location where rainfall is observed from the location where rainfall tends to intensify or weaken after being advected by the steering flow.

A major finding is that the spatial organization of GD is closely linked to the coastal–orographic setting of western Sumatra. The multi-year mean GD pattern shows that positive and negative GD are not randomly distributed, but tend to form organized structures around the coastal transition and the Bukit Barisan terrain. This indicates that the western coastal zone and the adjacent mountain slope act as important regions for precipitation modification. However, the result should not be interpreted as a simple elevation-controlled response. The strongest terrain does not always correspond directly to the strongest growth. Instead, precipitation growth and decay appear to depend on how the steering flow intersects the coastline, coastal plain, and mountain barrier.

The dominance of westerly and southwesterly steering flow emphasizes the role of the Indian Ocean sector in modulating precipitation evolution over Padang. These flow regimes transport

precipitation systems toward the western coast of Sumatra, allowing them to interact with the coastal boundary and the windward side of the Bukit Barisan range. Under these conditions, the spatial contrast between growth and decay becomes clearer, especially along the coastal–orographic corridor. This interpretation is consistent with the physical setting of western Sumatra, where rainfall is strongly influenced by land–sea interaction, diurnal convection, and orographic forcing.

The GD distribution also shows that precipitation evolution in this region is highly variable. Although the overall mean GD is close to neutral, the spread of GD values is large, indicating that individual precipitation systems can undergo substantial growth or decay. Therefore, the weak positive mean should not be interpreted as evidence of uniform rainfall intensification. Instead, it represents the net outcome of many contrasting growth and decay processes. This highlights the usefulness of the GD diagnostic: it can reveal whether rainfall systems tend to strengthen or weaken during their movement, even when the long-term average appears nearly balanced.

The flow-speed analysis refines this interpretation. The initial expectation might be that stronger flow would enhance orographic lifting and therefore produce stronger precipitation growth. However, the final composites show a more complex response. Under both westerly and southwesterly regimes, fast-flow conditions tend to produce broader negative GD over much of the coastal–orographic corridor. This suggests that stronger advection may reduce the residence time of precipitation systems over the terrain, limiting the time available for local growth and favoring more extensive weakening. In contrast, slow-flow conditions produce a more mixed GD pattern, indicating that weaker steering flow may allow precipitation systems to interact more gradually with local coastal and terrain-induced processes. Thus, flow speed does not simply amplify growth; it modulates the balance between growth, decay, and system displacement.

Temporal variability provides another important control on precipitation growth. The analysis of positive GD values shows that growth intensity varies across the diurnal cycle, with stronger growth generally appearing from late morning to afternoon. This timing is physically consistent with the development of daytime heating over land, enhanced boundary-layer instability, and local convergence near the coastal and orographic transition. The land–ocean separation further indicates that growth over land and ocean does not peak identically. Land growth is more strongly enhanced around midday, while ocean growth remains important during parts of the afternoon to evening period. This suggests that the timing of precipitation growth is influenced by the interaction between land heating, coastal circulation, and the broader steering flow.

The monthly variability of positive growth also indicates that the background environment changes across the annual cycle. The strongest full-domain growth occurs around August, while weaker values appear around December. Land growth is generally stronger during the mid-year months, whereas ocean growth becomes comparable to or stronger than land growth during

parts of the later wet-season period. This seasonal contrast suggests that the relative importance of land-based convective enhancement and oceanic precipitation growth varies throughout the year. However, because this analysis uses only positive GD values, the result should be interpreted as the conditional intensity of growth events rather than the frequency of rainfall occurrence.

Several limitations should be acknowledged. First, the ERA5 850-hPa wind field was used as an approximation of the steering flow. While this level represents lower-tropospheric advection reasonably well, it cannot fully capture storm-scale propagation, vertical wind shear, or local land–sea and mountain–valley circulations. Second, IMERG provides spatially continuous rainfall estimates, but satellite precipitation retrievals may contain uncertainties over coastal and complex terrain regions. In addition, the land–ocean mask is limited by the spatial resolution of the IMERG grid, so some coastal pixels may contain mixed land and ocean surfaces. Third, BMKG rain-gauge observations were used only as daily-scale observational support for IMERG rainfall accumulation and event interpretation. They were not used as direct validation of the 30-min GD fields because their temporal resolution is not equivalent to the sub-daily IMERG-based analysis.

Despite these limitations, the semi-Lagrangian GD framework provides a useful diagnostic for examining precipitation evolution in coastal–orographic terrain. The results show that precipitation growth and decay over Padang are shaped by multiple interacting factors: steering-flow direction, flow speed, land–sea contrast, diurnal timing, and seasonal background conditions. This framework therefore complements conventional rainfall climatology by identifying not only where rainfall occurs, but also where and under what conditions rainfall tends to intensify or weaken. Future work could improve this analysis by incorporating higher-resolution wind information, independent storm-motion estimates, higher-resolution regional reanalysis, or denser rain-gauge networks to better resolve storm-scale dynamics and validate sub-daily precipitation evolution.

5. Conclusions

This study investigated the growth and decay (GD) characteristics of precipitation over the Padang coastal–orographic region during 2020–2024 using a semi-Lagrangian framework based on IMERG Final Run V07B precipitation and ERA5 850-hPa steering flow. The approach allowed precipitation evolution to be examined along the estimated flow pathway, rather than only at fixed locations, thereby providing additional insight into where rainfall tends to intensify or weaken as it interacts with the coastal and mountainous environment of western Sumatra.

The results show that the spatial distribution of GD is strongly organized by the coastal–orographic setting. Positive GD tends to occur near the western coastal sector and the upstream side of the Bukit Barisan terrain, while weaker or negative GD is more evident farther inland and around elevated regions. This indicates that precipitation modification in the study area is

controlled not simply by terrain height, but by the interaction between steering flow, coastline orientation, and the steep topographic gradient.

The statistical and directional analyses further reveal that valid GD samples are most frequently associated with westerly and southwesterly flow regimes. These regimes represent onshore or oblique-onshore transport from the Indian Ocean toward western Sumatra and produce the clearest coastal-to-inland contrast in GD. However, flow speed modifies this response. Fast-flow conditions under the dominant W and SW regimes tend to produce broader negative GD, suggesting that stronger advection may reduce the residence time of rainfall systems over the coastal–orographic zone and favor weakening rather than widespread growth.

Temporal analysis of positive GD values indicates that precipitation growth is also modulated by diurnal and monthly variability. Growth intensity is generally enhanced from late morning to afternoon, with land and ocean sectors showing different timing characteristics. Monthly growth reaches its strongest full-domain value around August and weakens around December, indicating that seasonal background conditions influence the intensity of growth events. These findings suggest that precipitation evolution in the Padang region is governed by a combination of steering-flow direction, flow speed, land–sea contrast, diurnal timing, and seasonal variability.

Overall, the semi-Lagrangian GD framework provides a useful diagnostic for understanding precipitation evolution in complex coastal–orographic terrain. While IMERG and ERA5 allow consistent multi-year analysis, future work should incorporate higher-resolution wind information, independent storm-motion estimates, and denser observational networks to better resolve storm-scale dynamics and validate sub-daily growth–decay processes.

Declarations

Competing Interests

No, I declare that the authors have no competing interests as defined by Springer, or other interests that might be perceived to influence the results and/or discussion reported in this paper.

Data Availability

The GPM IMERG Final Run V07B precipitation data, ERA5 reanalysis data, and ETOPO1 topographic data used in this study are publicly available from their respective official data providers. The BMKG daily rain-gauge observations used to support the analysis are not publicly available due to institutional data restrictions, but may be made available from the corresponding author upon reasonable request and with permission from BMKG.

Acknowledgements

The authors acknowledge NASA/JAXA, ECMWF, NOAA, and BMKG for providing the datasets used in this study. The authors also thank the Meteorology Study Program, Sekolah Tinggi Meteorologi Klimatologi dan Geofisika, for academic support during the preparation of this research.

Research Funding

This research did not receive funding.

References

Amante, C., & Eakins, B. W. (2009). *ETOPO1 1 arc-minute global relief model: Procedures, data sources and analysis*. NOAA National Geophysical Data Center. https://doi.org/10.7289/V5C8276M

Hamada, J.-I., Yamanaka, M. D., Mori, S., Tauhid, Y. I., & Sribimawati, T. (2008). Differences of rainfall characteristics between coastal and interior areas of central western Sumatera, Indonesia. *Journal of the Meteorological Society of Japan, 86*(5), 593–611. https://doi.org/10.2151/jmsj.86.593

Hersbach, H., Bell, B., Berrisford, P., Hirahara, S., Horányi, A., Muñoz-Sabater, J., Nicolas, J., Peubey, C., Radu, R., Schepers, D., Simmons, A., Soci, C., Abdalla, S., et al. (2020). The ERA5 global reanalysis. *Quarterly Journal of the Royal Meteorological Society, 146*(730), 1999–2049. https://doi.org/10.1002/qj.3803

Huffman, G. J., Bolvin, D. T., Braithwaite, D., Hsu, K., Joyce, R., Kidd, C., Nelkin, E. J., Sorooshian, S., Stocker, E. F., Tan, J., Wolff, D. B., & Xie, P. (2020). Integrated Multi-satellitE Retrievals for the Global Precipitation Measurement mission. In V. Levizzani, C. Kidd, D. B. Kirschbaum, C. D. Kummerow, K. Nakamura, & F. J. Turk (Eds.), *Satellite precipitation measurement* (pp. 343–353). Springer. https://doi.org/10.1007/978-3-030-24568-9_19

Kim, K., Tsai, C.-L., & Lee, G. (2025). A radar-based investigation of precipitation growth and decay in South Korea. *Quarterly Journal of the Royal Meteorological Society, 151*, e4988. https://doi.org/10.1002/qj.4988

Marzuki, M., Yusnaini, H., Ramadhan, R., Tangang, F., Amirudin, A. A. B., Hashiguchi, H., Shimomai, T., & Vonnisa, M. (2022a). Characteristics of precipitation diurnal cycle over a mountainous area of Sumatra Island including MJO and seasonal signatures based on the 15-year optical rain gauge data, WRF model and IMERG. *Atmosphere, 13*(1), 63. https://doi.org/10.3390/atmos13010063

Marzuki, M., Yusnaini, H., Tangang, F., Muharsyah, R., Vonnisa, M., & Harmadi, H. (2022b). Land–sea contrast of diurnal cycle characteristics and rain event propagations over Sumatra according

to different rain duration and seasons. *Atmospheric Research, 270*, 106051. https://doi.org/10.1016/j.atmosres.2022.106051

Mori, S., Hamada, J.-I., Tauhid, Y. I., Yamanaka, M. D., Okamoto, N., Murata, F., Sakurai, N., Hashiguchi, H., & Sribimawati, T. (2004). Diurnal land–sea rainfall peak migration over Sumatera Island, Indonesian Maritime Continent, observed by TRMM satellite and intensive rawinsonde soundings. *Monthly Weather Review, 132*(8), 2021–2039. https://doi.org/10.1175/1520-0493(2004)132<2021:DLRPMO>2.0.CO;2

Yusnaini, H., Marzuki, M., Ramadhan, R., Ilham, R., Vonnisa, M., & Hashiguchi, H. (2024). Land–sea contrast of vertical structure of precipitation over Sumatra revealed by GPM DPR observations. *Atmospheric Research, 309*, 107555. https://doi.org/10.1016/j.atmosres.2024.107555